

# Heterogeneous Photodegradation of Pentachlorophenol and Iron Cycling with Goethite, Hematite and Oxalate under UVA Illumination

Qing Lan <sup>a, b, d</sup>, Fang-bai Li <sup>b, \*</sup>, Cui-xiang Sun <sup>b</sup>, Cheng-shuai Liu <sup>b</sup>, Xiang-zhong Li <sup>c</sup>

<sup>a</sup> *Guangzhou Institute of Geochemistry, Chinese Academy of Sciences, Guangzhou 510640, PR China*

<sup>b</sup> *Guangdong Key Laboratory of Agricultural Environment Pollution Integrated Control, Guangdong Institute of Eco-Environmental and Soil Sciences, Guangzhou 510650, PR China*

<sup>c</sup> *Department of Civil and Structural Engineering, The Hong Kong Polytechnic University, Hong Kong, PR China*

<sup>d</sup> *Graduate University of Chinese Academy of Sciences, Beijing 100039, PR China*

## Abstract

Heterogeneous photodegradation of pentachlorophenol (PCP) in the goethite ( $\alpha$ -FeOOH) and hematite ( $\alpha$ -Fe<sub>2</sub>O<sub>3</sub>) systems with oxalate under UVA illumination was investigated. The PCP degradation, dechlorination and detoxification, in terms of Microtox acute toxicity, were achieved to the higher efficiency in the hematite suspension than in the goethite suspension. The optimal initial concentration of oxalic acid ( $C_{ox}^0$ ) for the PCP degradation with goethite and hematite under the experimental conditions was found to be 1.2 mM, since sufficient Fe(III) as Fe(C<sub>2</sub>O<sub>4</sub>)<sub>3</sub><sup>3-</sup> and Fe(II) as Fe(C<sub>2</sub>O<sub>4</sub>)<sub>2</sub><sup>2-</sup> can be formed at  $C_{ox}^0 \geq 1.2$  mM. The main intermediates of PCP degradation were identified through GC-MS, HPLC and IC analyses. It was found that the cycling process between Fe(III) and Fe(II) in both the goethite and hematite systems occurred more vigorously at the initial stage and gradually became gentle, while the rate of PCP photodegradation varied from fast to slow during the reaction time. Furthermore, the formation of H<sub>2</sub>O<sub>2</sub> during photoreaction was also studied to explore its effects on the photodegradation and the iron cycling processes.

**Keywords:** Heterogeneous photodegradation; pentachlorophenol; iron cycle; goethite; hematite; oxalate

---

\*Corresponding author phone: 86-20-87024721; fax: 86-20-87024123; e-mail: [cefbli@soil.gd.cn](mailto:cefbli@soil.gd.cn) and [cefbli@hotmail.com](mailto:cefbli@hotmail.com) (Dr. Fangbai Li).

## 27 1. Introduction

28 Iron, as the fourth most abundant element of the earth's crust, is rich in the  
29 environment. Oxalic acid, mainly secreted by plant roots [1] or formed by incomplete  
30 combustion of hydrocarbons [2, 3], is ubiquitous in soil, water and atmosphere. In nature,  
31 iron, oxalic acid, and sunlight can establish a homogeneous photo-Fenton-like system  
32 where iron exists in a dissolved form or a heterogeneous photo-Fenton-like system where  
33 iron is in a solid form. The heterogeneous Fe(III)-oxalate system should be more  
34 applicable to the natural environment, because the iron species are mostly present as  
35 amorphous or (hydr)oxides. In the 1990s several research groups [4-8] studied the  
36 mechanisms of iron (hydr)oxides dissolution in aqueous oxalate solution. Sulzberger's  
37 group explored the degradation of diiron in a goethite-oxalate system irradiated by UV  
38 [9]. Our group studied the effects of reaction conditions and the distribution of various  
39 iron species in the iron oxide-oxalate-UV system [10-13]. It is generally accepted that the  
40 reaction mechanisms of such a heterogeneous system include several critical processes.  
41 The chemical adsorption of oxalic acid first occurs on the surface of iron oxide leading to  
42 the formation of Fe-oxalate complexes, and simultaneously the non-reductive/reductive  
43 dissolution of iron oxide takes place [9-13]. Light irradiation can greatly enhance the  
44 reductive dissolution of Fe(III)-oxalate complexes, yielding Fe(II) and oxalate radical  
45  $(C_2O_4)^{\bullet-}$  [6-13]. In the presence of  $O_2$ , the most reactive oxidant,  $\bullet OH$ , can be obtained by  
46 the Fenton reaction of  $H_2O_2$  with Fe(II), and iron cycling involving a series of active  
47 radicals can take place in the system [2-3, 13-15].

48 Compared with classical photo-Fenton systems ( $Fe^{2+}$  or  $Fe^{3+}/H_2O_2$ ), the  
49 photo-Fe-oxalate system can form  $H_2O_2$  in situ, and has the higher efficiency for the  
50 degradation of organic compounds [1, 14, 16]. While the homogeneous Fe-oxalate  
51 systems have been explored in many previous studies [1-3, 14-20], the heterogeneous  
52 Fe-oxalate systems, which do not easily bring about the secondary contamination of

53 abundant dissolved Fe ions in practical applications, have only received scant attention.

54 In the heterogeneous system, various iron (hydr)oxides demonstrate different  
55 dissolution properties [8]. The preparation method and intrinsic structure largely  
56 influence the activities of iron oxides [21-23]. Doping agents also significantly affect the  
57 photocatalytic activity of iron oxides [24, 25]. In the irradiated heterogeneous iron  
58 oxide-oxalate system, iron cycling, which happens both heterogeneously and  
59 homogeneously [6-8, 10], is essential because it produces H<sub>2</sub>O<sub>2</sub> and •OH continuously.  
60 However, studies of the dissimilarities of iron oxides with different crystal structures in  
61 degrading contaminants and especially the generation of H<sub>2</sub>O<sub>2</sub> and the different Fe  
62 species are scant, but are very important for understanding such complicated  
63 heterogeneous reactions.

64 In the present study, pentachlorophenol (PCP) was chosen as a probe pollutant because  
65 of its persistence in the environment and high toxicity due to the five chlorine atoms in  
66 its structure. The aim of this study was at comparing the activities of two iron oxides  
67 (goethite and hematite) in degrading PCP with oxalate under UV illumination, and  
68 investigating the formation of H<sub>2</sub>O<sub>2</sub> and the adsorbed/dissolved Fe species cycling. In  
69 addition, the dechlorination, detoxification (Microtox acute toxicity) and intermediates of  
70 PCP were also investigated.

71

## 72 **2. Experiments and Methods**

### 73 **2.1 Chemicals**

74 PCP (98%) chemical was purchased from Aldrich, USA. Tetrachloro-*p*-benzoquinone  
75 (99%), tetrachloro-*o*-benzoquinone (97%), methanol (HPLC grade) and hexane (HPLC  
76 grade) chemicals were obtained from Acros, Belgium. Other chemicals with analytical  
77 grade were purchased from Guangzhou Chemical Co. China. All the chemicals were used  
78 as received except acetic anhydride, which was redistilled for GC/MS analysis.

79 Deionized water (18.2 mΩ cm) from an ultrapure water system (Easy Pure<sup>®</sup> II RF/UV,  
80 USA) was used in all experiments. Goethite ( $\alpha$ -FeOOH) and hematite ( $\alpha$ -Fe<sub>2</sub>O<sub>3</sub>) powders  
81 were synthesized according to the procedures previously reported [26]. While their  
82 composition and crystal structures were confirmed by X-ray powder diffraction (XRD),  
83 their specific surface areas were measured to be 32.3 and 29.4 m<sup>2</sup> g<sup>-1</sup>, respectively by the  
84 Brunauer–Emmett–Teller (BET) method..

85

## 86 **2.2 Photochemical experiment**

87 Aqueous PCP stock solution (0.075 mM) was prepared with 1.0% (v/v) ethanol and  
88 stored in a dark-brown glass bottle to avoid any photochemical reaction. In all  
89 photodegradation experiments, aqueous suspensions contained the same initial PCP  
90 concentration (0.0375 mM) and the same iron oxide content (0.4 g L<sup>-1</sup>), but different  
91 initial concentrations of oxalic acid (C<sup>0</sup><sub>ox</sub>). Ethanol was used to prepare the above  
92 aqueous PCP solutions and its concentration in all experiments was kept strictly at 0.5%  
93 as it is an •OH scavenger. It is believed that the ethanol would affect PCP degradation to  
94 a similar extent in all experiments, but should not affect the pattern of PCP degradation  
95 kinetics. All experiments were carried out in a photochemical reactor system described  
96 with details previously [10] at 30°C using a thermostatted water bath. Prior to UV light  
97 irradiation, adsorption/desorption equilibrium in the aqueous PCP suspension was  
98 established in the dark for 30 min. The suspension was continuously stirred by a  
99 magnetic stirrer and bubbled with air throughout each experiment. The water samples for  
100 HPLC, IC and GC-MS analyses were taken at various time intervals and then were  
101 centrifuged at 4500 rpm for 25 min, and further filtered through a 0.45 μm filter before  
102 injecting into the analytical instruments.. The initial pH of suspensions was adjusted to  
103 3.5 using NaOH or HClO<sub>4</sub> solution.

104

### 105 2.3 Analysis

106 PCP and its reaction intermediates were determined by HPLC (Waters 1525/2487)  
107 with an Xterra C18 reverse-phase column. For PCP analysis, a mobile phase containing  
108 1% acetic acid in water/methanol (20:80 v/v) mixed solvent flew at a rate of 1.0 mL min<sup>-1</sup>.  
109 The column temperature was set at 35 °C and UV detection was set at 295 nm. Following  
110 the analytical procedure described by Oturan et al. [27], tetrachloro-*p*-benzoquinone and  
111 tetrachloro-*o*-benzoquinone were identified by comparing their retention times with  
112 internal standards. The mobile phase and flow rate were the same as the noted above, but  
113 the ratio of 1% acetic acid in water to methanol was 25:75 (v/v), and the column  
114 temperature and the detector wavelength were set at 30 °C and 280 nm, respectively.

115 The concentrations of oxalic acid and chloride ions were determined by ion  
116 chromatography (IC Dionex ICS-90) with a mobile phase of aqueous 1.0 mM  
117 NaHCO<sub>3</sub>-8.0 mM Na<sub>2</sub>CO<sub>3</sub> solution at a flow rate of 1.0 mL min<sup>-1</sup>. An LC-10A system  
118 (Shimadzu) with IC-A3 column was used to identify the intermediate products (HCOOH  
119 and CH<sub>3</sub>COOH) with a mobile phase of 2.5 mM phthalic acid and 2.4 mM Tris solution  
120 at a flow rate of 1.2 mL min<sup>-1</sup> and 40 °C.

121 H<sub>2</sub>O<sub>2</sub> in aqueous solution was measured using an H<sub>2</sub>O<sub>2</sub> analyzer (Lovibond-ET8600,  
122 Germany), in which Lovibond reagent was reacted with H<sub>2</sub>O<sub>2</sub> in a 10 mL vessel to form a  
123 colored solution, and the concentration of H<sub>2</sub>O<sub>2</sub> was determined photometrically at 528  
124 nm with a detection limit of 0.05 mg L<sup>-1</sup>. The Lovibond reagent was first added in the  
125 vessel before the sample was taken from the photoreactor. At each time interval, 10 mL  
126 of reaction solution was sampled and immediately filtered through a 0.45 μm filter before  
127 it was placed into the vessel, and the concentration of H<sub>2</sub>O<sub>2</sub> in the filtrate was measured  
128 at once. After this procedure was completed for one min, the validity of H<sub>2</sub>O<sub>2</sub>  
129 concentration was ensured.

130 A GC-MS (Thermo Trace-DSQ-2000) system with electron ionization and an Agilent  
131 silicon capillary column (0.25 mm × 30 m) was used to determine other products from

132 PCP degradation in which the samples were pretreated by extraction as the described  
133 previously [28, 29].

134 A Microtox analyzer (Strategic Diagnostics Inc., U.S. Model 500) was used to measure  
135 the Microtox acute toxicity of samples, in which the relative degree of sample toxicity is  
136 expressed by the percentage of light loss. The details of the measurement method can be  
137 found elsewhere [13].

138 Dissolved Fe(II) was measured colorimetrically by the ferrozine method and total  
139 dissolved iron was determined in the same way after adding 10% OHNH<sub>3</sub>Cl to reduce all  
140 Fe(III)(aq) to Fe(II)(aq). The adsorbed Fe(III)/Fe(II) on the surface of iron oxide was  
141 extracted by 0.1 M HCl solution with stirring for 30 min in the dark prior to the above  
142 analyses. Since no iron ion was detected in the  $\alpha$ -FeOOH/ $\alpha$ -Fe<sub>2</sub>O<sub>3</sub> suspensions in the  
143 absence of oxalic acid under this extraction condition, it indicated that the fixed iron of  
144  $\alpha$ -FeOOH/ $\alpha$ -Fe<sub>2</sub>O<sub>3</sub> should not be extracted to interfere with the measurement of adsorbed  
145 Fe species. To avoid the oxidation of Fe(II), the sample filtered through the 0.45  $\mu$ m filter  
146 was measured promptly after sample collection. In the measurement of Fe(III), several  
147 minutes were needed to allow complete reduction of Fe(III) to take place before addition  
148 of the buffer and ferrozine.

149

### 150 **3. Results and Discussion**

#### 151 **3.1 Photodegradation of PCP**

152 The experimental results of PCP photodegradation under different conditions are  
153 presented in Figure 1. The results showed that 30-68% of PCP was removed after 1 h  
154 reaction time in the  $\alpha$ -FeOOH suspension with different initial concentrations of oxalic  
155 acid ( $C_{ox}^0$ ) (Figure 1A), which was much lower than that (49-83%) in the  $\alpha$ -Fe<sub>2</sub>O<sub>3</sub>  
156 suspension (Figure 1B). In the absence of oxalic acid, PCP was only slightly degraded by  
157 direct photolysis at below 370 nm [28]. The results demonstrate that the presence of

158 oxalic acid greatly enhanced PCP degradation and an optimal  $C_{\text{ox}}^0$  in the  $\alpha$ -FeOOH and  
159  $\alpha$ -Fe<sub>2</sub>O<sub>3</sub> systems was found to be around 1.2 mM. With this optimal  $C_{\text{ox}}^0$ , 68 and 83% of  
160 PCP was photocatalytically degraded after 1 h in the  $\alpha$ -FeOOH and  $\alpha$ -Fe<sub>2</sub>O<sub>3</sub> systems,  
161 respectively.

162 The Fe species should play an important role in the PCP degradation because various  
163 Fe species have different photoactivity [1, 9, 18]. For example, Fe(III) in the form of  
164  $\text{Fe}(\text{C}_2\text{O}_4)_2^-$  and  $\text{Fe}(\text{C}_2\text{O}_4)_3^{3-}$  can be more efficiently photolyzed to Fe(II) than as other  
165 species [1, 9, 19], and Fe(II) as  $\text{Fe}(\text{C}_2\text{O}_4)_2^{2-}$  can react with H<sub>2</sub>O<sub>2</sub> to form •OH at a much  
166 faster rate than that as Fe<sup>2+</sup> [1, 9, 19]. According to the method described by Panias et al.  
167 [4], the fractions of different Fe species in iron oxide-oxalate suspensions can be  
168 calculated as the functions of pH and oxalic acid concentration. Using the tested pH  
169 values and oxalic acid concentrations during the experiments, the changes in distribution  
170 of different Fe(III)/Fe(II) species during the reaction time in the  $\alpha$ -FeOOH or  $\alpha$ -Fe<sub>2</sub>O<sub>3</sub>  
171 suspension were calculated accordingly [13]. In the  $\alpha$ -FeOOH or  $\alpha$ -Fe<sub>2</sub>O<sub>3</sub> suspension  
172 during the photoreaction, the Fe(III) species  $\text{Fe}(\text{C}_2\text{O}_4)_2^-$  and/or  $\text{Fe}(\text{C}_2\text{O}_4)_3^{3-}$  with high  
173 photoactivity were found to be the dominant species (> 90%) at different  $C_{\text{ox}}^0$ . For Fe(II)  
174 species in the two suspensions, it was found that at  $C_{\text{ox}}^0 = 0.4$  mM, the Fe<sup>2+</sup> species with  
175 low photoactivity was the dominant species (> 60%). At  $0.4 \text{ mM} < C_{\text{ox}}^0 < 1.2 \text{ mM}$ , the  
176 amounts of Fe<sup>2+</sup> and  $\text{Fe}(\text{C}_2\text{O}_4)_2^{2-}$  were similar with a total Fe(II) species fraction of >  
177 90%, and at  $C_{\text{ox}}^0 \geq 1.2 \text{ mM}$ ,  $\text{Fe}(\text{C}_2\text{O}_4)_2^{2-}$  became the dominant Fe(II) species (> 80%).  
178 Consequently, it is reasonable to assume that at  $C_{\text{ox}}^0 = 1.2 \text{ mM}$  in the  $\alpha$ -FeOOH or  
179  $\alpha$ -Fe<sub>2</sub>O<sub>3</sub> suspension, the two species of Fe (III) as  $\text{Fe}(\text{C}_2\text{O}_4)_3^{3-}$  and Fe(II) as  $\text{Fe}(\text{C}_2\text{O}_4)_2^{2-}$   
180 with high photoactivity were formed to a sufficient extent to cause PCP degradation.  
181 However, since oxalic acid itself was also a scavenger of •OH, the reaction rate of PCP  
182 degradation decreased at  $C_{\text{ox}}^0 > 1.2 \text{ mM}$ .

183 [FIGURE 1]

184

### 185 **3.2 Dechlorination and detoxification of PCP**

186 The ratio of dechlorination (%) was calculated as  $[Cl^-]/[T-Cl_0]$  where  $[Cl^-]$  is the  
187 concentration of chloride released from PCP degradation and  $[T-Cl_0]$  is the stoichiometric  
188 concentration of organic chlorine in PCP. **Figure 2** shows the rates of dechlorination in  
189 the two iron oxide systems with oxalate under UVA illumination. After 1 h reaction  
190 time, the dechlorination in the  $\alpha$ -FeOOH system was achieved by 2-16% (**Figure 2A**),  
191 which was much lower than that in the  $\alpha$ -Fe<sub>2</sub>O<sub>3</sub> system (7-28%) (**Figure 2B**). The amount  
192 of released chloride was much higher in the presence than in the absence of oxalic acid.  
193 The highest rate of dechlorination was obtained at the optimal  $C_{ox}^0$  of 1.2 mM in both the  
194  $\alpha$ -FeOOH and  $\alpha$ -Fe<sub>2</sub>O<sub>3</sub> suspensions. Furthermore, as the described previously [13,] the  
195 dechlorination reaction continued in the reactions with intermediate products after 1 h  
196 reaction time (data not shown here). Oturan *et al.* reported a similar phenomenon for PCP  
197 degradation in an electro-Fenton system [27]. These results may indicate that the  
198 cleavage of Cl-C bonds due to •OH attack has no preference compared to other  
199 degradation reactions in the system.

200 The data in **Figure 3** confirmed the detoxification of PCP in terms of light loss  
201 determined with the Microtox analysis. At  $C_{ox}^0 = 1.2$  mM, the ratios of light loss after 1 h  
202 reaction decreased from 83 and 84% for the  $\alpha$ -FeOOH and  $\alpha$ -Fe<sub>2</sub>O<sub>3</sub> systems to 54 and  
203 46%, Respectively. It is also proposed that the detoxification reaction continued with  
204 extension of the reaction time beyond 1 h as reported previously [13]. In addition, it is  
205 apparent that the results of dechlorination and detoxification were consistent in line with  
206 the PCP degradation, indicating that PCP was more efficiently degraded in the  $\alpha$ -Fe<sub>2</sub>O<sub>3</sub>  
207 system than that in the  $\alpha$ -FeOOH system.

208 **[FIGURE 2]**

209 **[FIGURE 3]**

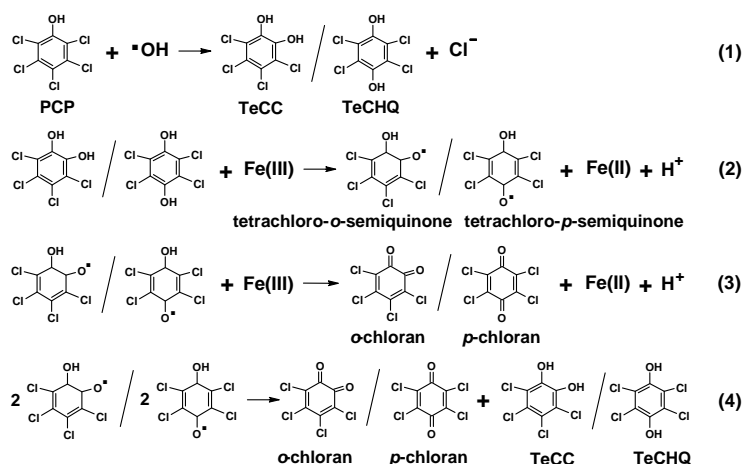


210

### 211 3.3 Intermediates from PCP degradation

212 Although PCP was degraded in the  $\alpha$ -FeOOH and  $\alpha$ -Fe<sub>2</sub>O<sub>3</sub> systems at different rates,  
 213 the same intermediates were identified in the two systems with oxalic acid under UVA  
 214 illumination, including tetrachlorocatechol (TeCC) and  
 215 2,3,5,6-tetrachloro-1,4-hydroquinone (TeCHQ) by GC-MS, tetrachloro-*o*-benzoquinone  
 216 (*o*-chloranil) and tetrachloro-*p*-benzoquinone (*p*-chloranil) by HPLC, and HCOOH and  
 217 CH<sub>3</sub>COOH by IC.

218 Hydroquinone has been found to be a catalyst in the Fenton reaction to rapidly reduce  
 219 Fe(III) to Fe(II) through an intermediate cycling by generation of a semiquinone product  
 220 [30, 31], in which, hydroquinone reduces Fe(III) to form semiquinone and the  
 221 semiquinone reduces Fe(III) to form quinone, while hydroquinone and quinone can be  
 222 renewably formed by the dismutation of semiquinone [30, 31]. Such a intermediate  
 223 cycling involving the reduction of Fe(III) can combine with the iron cycling of the  
 224 system to accelerate the generation of Fe (II) and active species [31]. The intermediate  
 225 cycling is described by equations (1)-(4), and the results in section 3.5 showed that more  
 226 H<sub>2</sub>O<sub>2</sub> was formed in the presence than in the absence of PCP, indicating the existence of  
 227 the intermediate promotion mechanism involving the iron cycling.



228

229 The above intermediate cycling can explain to some extent why production of  
 230 Cl<sub>3</sub>C<sub>6</sub>(OH)<sub>3</sub> was not detected, because the oxidation to tetrachloro benzoquinone is more

231 favorable compared with further hydroxylation of the ring in such systems. Augusti *et al.*  
232 [32] reported similar results for chlorobenzene degradation by Fenton's reagent. The  
233 formation of organic acids with small molecule such as HCOOH and CH<sub>3</sub>COOH  
234 confirmed that PCP was mineralized to some extent after its aromatic ring was  
235 broken after 1 h reaction time.

236 The control experiments showed that CH<sub>3</sub>COOH was formed by oxidation of PCP  
237 and/or ethanol. Since the formation and degradation of intermediate products occurred at  
238 the same time, it was difficult to quantify the contribution of PCP to the fraction of  
239 CH<sub>3</sub>COOH formation. Two other intermediates, tetrachloro-*p*-benzoquinone (*p*-chloranil)  
240 and HCOOH, were quantified as shown in Figure 4. It was found that the concentrations  
241 of the two intermediates in the α-FeOOH system were significantly higher than those in  
242 the α-Fe<sub>2</sub>O<sub>3</sub> system. The results in sections 3.1 and 3.5 showed that the both rates of PCP  
243 degradation and H<sub>2</sub>O<sub>2</sub> formation in the α-FeOOH suspension were significantly lower  
244 than those in the α-Fe<sub>2</sub>O<sub>3</sub> suspension. All of these results indicated that more active  
245 substances could be generated in the α-Fe<sub>2</sub>O<sub>3</sub> suspension to degrade the intermediates  
246 from PCP degradation. The shorter lifetime of these intermediates resulted in less  
247 accumulation in the α-Fe<sub>2</sub>O<sub>3</sub> suspension.

248 [FIGURE 4]

249

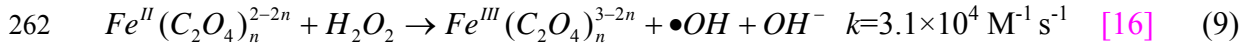
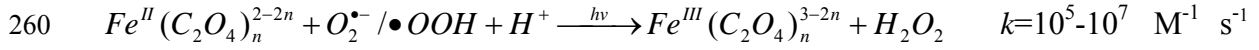
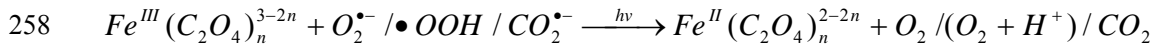
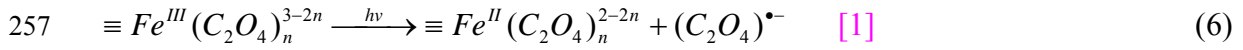
### 250 3.4 Iron cycling during PCP degradation

251 Iron cycling is a key step in the Fenton reaction to continuously form H<sub>2</sub>O<sub>2</sub> and •OH  
252 in an iron oxide-oxalate system, either in the dark or under light irradiation, as shown  
253 below [4-8]:

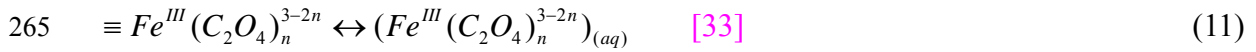
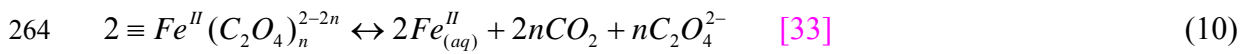
254 In the dark:



256 Under light irradiation:



263 In addition, the interface transfer process should be involved throughout the iron cycling:



266 The mechanism of iron cycling in the iron oxide-oxalate-UV system **in the presence of**  
 267 **PCP**[delete?] is presented in **Scheme 1**. This cycling takes place simultaneously both on  
 268 the surface of iron oxide and in the bulk solution. The hydroquinone/quinone  
 269 intermediates of PCP can catalyze this cycling as the discussed above (**Eqs. (1)-(4)**). The  
 270 interface transfer processes (**Eqs. (10)-(11)**) of Fe(III)/Fe(II) play an important role in the  
 271 interaction between surface reaction and solution reaction.

272 To quantitatively study the iron cycling during PCP degradation, the concentrations of  
 273 adsorbed and dissolved Fe(III)/Fe(II) versus reaction time were determined as shown in  
 274 **Figure 5**. The concentration of adsorbed/dissolved Fe(III)/Fe(II) was mainly in the range  
 275 0.01-0.10 mM, which was much lower than the stoichiometric concentration  
 276 corresponding to 0.4 g L<sup>-1</sup> of  $\alpha$ -FeOOH/ $\alpha$ -Fe<sub>2</sub>O<sub>3</sub> and the initial concentration of oxalic  
 277 acid used. However, Zuo et al. [2-3] reported that H<sub>2</sub>O<sub>2</sub> and  $\bullet$ OH could be formed at  
 278 much lower concentrations of Fe(III) (1  $\mu$ M) and oxalate (5  $\mu$ M), indicating that the  
 279 amounts of Fe(III)/Fe(II) in our experiments were sufficient to form H<sub>2</sub>O<sub>2</sub> and  $\bullet$ OH.

280 After 30 min of adsorption/desorption equilibration in the dark, the concentration of  
 281 adsorbed Fe(III) increased with the increase of C<sub>ox</sub><sup>0</sup> in both the  $\alpha$ -FeOOH and  $\alpha$ -Fe<sub>2</sub>O<sub>3</sub>

282 systems. Only small amounts of dissolved Fe(III) and Fe(II) were formed by desorption  
283 of surface Fe(III)-oxalate complexes (Eq. (11)) and the slow reductive dissolution in the  
284 dark (Eq. (5)).

285 Figure 5 indicates that the amounts of all Fe species during photodegradation of PCP  
286 varied greatly in the initial stages of reaction, which might result from the fast redox  
287 cycling of Fe(III)/Fe(II) with vigorous interface transfer. It is known that light irradiation  
288 can greatly enhance the photochemical electron transfer of Fe(III)-oxalate complexes (Eq.  
289 (6)-(9)) [5-8]. In the late stage of reaction, the variation of the amounts of the different Fe  
290 species declined significantly, which might result from the loss of oxalic acid and the  
291 increase of pH. Correspondingly, as shown in Figure 1, the degradation of PCP in the  
292  $\alpha$ -FeOOH or  $\alpha$ -Fe<sub>2</sub>O<sub>3</sub> suspension had the same pattern of rapid degradation in the initial  
293 stage and gradually decreasing degradation rate in the later stage.

294 In the study [35], different iron oxides with almost the same concentration of total  
295 dissolved Fe showed different activities toward degradation of mordant yellow 10 (MY  
296 10) in the iron oxide-H<sub>2</sub>O<sub>2</sub> suspension. In this study, it was found that the concentrations  
297 of dissolved Fe(III)/Fe(II) in the  $\alpha$ -FeOOH system were higher than in the  $\alpha$ -Fe<sub>2</sub>O<sub>3</sub>  
298 system during the reaction time as shown in Figure 5. However, PCP degradation in the  
299  $\alpha$ -FeOOH system was slower than in the  $\alpha$ -Fe<sub>2</sub>O<sub>3</sub> system. These results indicated that the  
300 amount of dissolved iron is not a rate-determining factor in relation to the activity of the  
301 iron oxides with different crystal structures. The exact mechanisms determining the  
302 activity of different iron oxides may involve their specific surface characters and the  
303 specific properties of target pollutants that need to be explored in further research.

304 In these heterogeneous iron oxide-oxalate systems, the dissolved Fe(II)/Fe(III) resulted  
305 from the redox reaction of Fe(III)/Fe(II) in solution, and also the interface transfer of  
306 Fe(II)/Fe(III) on the surface. As shown in Figure 5, it is interesting that the amounts of  
307 adsorbed Fe(II)/Fe(III) in the  $\alpha$ -FeOOH or  $\alpha$ -Fe<sub>2</sub>O<sub>3</sub> system remained almost constant

308 during the late stage of reaction, indicating that the interface transfer process of  
309 Fe(II)/Fe(III) from surface to solution became slow due to the consumption of oxalic acid  
310 with pH increase, and might be a relatively slow process during the iron cycling.  
311 Sulzberger *et al.* and Banwart *et al.* noted that the interface process of detachment of  
312 Fe(II) from the surface was the rate-determining step in an iron oxide-oxalate-UV system  
313 [8-9, 36]. The results of this study should provide useful information to better understand  
314 the role of the interface transfer process during iron cycling in such heterogeneous  
315 systems.

316 [SCHEME 1]

317 [FIGURE 5]

318

### 319 **3.5 Formation of hydrogen peroxide.**

320 The most reactive oxidant,  $\bullet\text{OH}$ , is obtained through the  $\text{H}_2\text{O}_2$  reaction with Fe(II),  
321 while  $\text{H}_2\text{O}_2$  is mainly generated by the reaction of Fe(II) with  $\text{O}_2^{\bullet-}/\bullet\text{OOH}$  and the  
322 dismutation of  $\text{O}_2^{\bullet-}/\bullet\text{OOH}$  in the presence of  $\text{O}_2$  [1-3]. The concentration of  $\text{H}_2\text{O}_2$  in the  
323 system depends on both the rates of its generation and consumption. The more rapid is  
324 iron cycling, the greater amount of  $\text{H}_2\text{O}_2$  can be formed. The variation of  $\text{H}_2\text{O}_2$   
325 concentration vs. reaction time in the  $\alpha\text{-FeOOH}$  and  $\alpha\text{-Fe}_2\text{O}_3$  suspensions is presented in  
326 Figure 6.

327 In the absence of oxalic acid,  $\text{H}_2\text{O}_2$  was not detected during 60 min in the  $\alpha\text{-FeOOH}$  or  
328  $\alpha\text{-Fe}_2\text{O}_3$  system. In the presence of oxalic acid,  $\text{H}_2\text{O}_2$  was detected at a significant level  
329 between 0.1-1.2  $\text{mg L}^{-1}$  in the  $\alpha\text{-FeOOH}$  suspension (Figure 6A) and 1.2-3.0  $\text{mg L}^{-1}$  in  
330 the  $\alpha\text{-Fe}_2\text{O}_3$  suspension (Figure 6B). In both the  $\alpha\text{-FeOOH}$  and  $\alpha\text{-Fe}_2\text{O}_3$  systems, more  
331  $\text{H}_2\text{O}_2$  could be formed in the presence than in the absence of PCP at  $C_{\text{ox}}^0 = 1.2 \text{ mM}$ , and  
332 the concentrations of  $\text{H}_2\text{O}_2$  at  $C_{\text{ox}}^0 \geq 1.2 \text{ mM}$  were much higher than at  $C_{\text{ox}}^0 = 0.4 \text{ mM}$ . It  
333 was apparent that the concentration of  $\text{H}_2\text{O}_2$  in the  $\alpha\text{-Fe}_2\text{O}_3$  system was significantly

334 higher than that in the  $\alpha$ -FeOOH system.

335 The above results may explain why PCP was more effectively photodegraded in the  
336  $\alpha$ -Fe<sub>2</sub>O<sub>3</sub> system. In addition, the above results to a certain extent confirmed that the  
337 hydroquinone intermediates could accelerate iron cycling and promote the formation of  
338 active compounds as discussed in sections 3.3 and 3.4.

339 The Fe(III)-oxalate complexes are initially formed by the adsorption of oxalic acid [9,  
340 13]. Then the photo-reduction of Fe(III)-oxalate complexes can generate H<sub>2</sub>O<sub>2</sub> and a  
341 series of active radicals [1-3]. Thus, the amount of oxalic acid adsorption on the surface  
342 of iron oxide directly influenced the formation of H<sub>2</sub>O<sub>2</sub>. However, the adsorption abilities  
343 of different iron oxides are different due to different surface properties and crystal  
344 structures.

345 Recently, we systematically studied the adsorption behavior of oxalic acid on the  
346 surface of different iron oxides, including some important and effect factors. It was found  
347 that the ability of  $\alpha$ -Fe<sub>2</sub>O<sub>3</sub> to adsorb oxalic acid was much stronger than that of  $\alpha$ -FeOOH,  
348 and the adsorption of oxalic acid approached its maximum amount at about  $C_{ox}^0 = 1.2$   
349 mM on both iron oxides, which is consistent with the results of H<sub>2</sub>O<sub>2</sub> formation in the  
350 present study. The detailed results of these adsorption experiments will be reported in  
351 another paper.

352 [FIGURE 6]

353

#### 354 4. Conclusions

355 68 and 83% of PCP were photodegraded after 1 h reaction at  $C_{ox}^0 = 1.2$  mM in aqueous  
356 goethite and hematite suspensions, respectively. Dechlorination and detoxification  
357 (Microtox acute toxicity) of PCP were also achieved to a greater extent in the hematite  
358 suspension than in the goethite suspension, indicating that hematite has the higher  
359 activity than goethite for PCP degradation in such an iron oxide-oxalate system under

360 UVA illumination. The experiments further confirmed that more H<sub>2</sub>O<sub>2</sub> could be formed in  
361 the hematite system than in the goethite system due to the more rapid iron cycling, which  
362 is beneficial to enhance the PCP degradation.

363

### 364 **Acknowledgment**

365 The authors appreciate the financial support by the National Science Foundation of China  
366 (No. 40771105).

367

### 368 **Literature Cited**

- 369 [1] M.E. Balmer, B. Sulzberger, Atrazine degradation in irradiated iron/Oxalate systems:  
370 effects of pH and oxalate. *Environ. Sci. Technol.* 33 (1999) 2418-2424.
- 371 [2] Y.G. Zuo, J. Hoigne, Evidence for photochemical formation of H<sub>2</sub>O<sub>2</sub> and oxidation of  
372 SO<sub>2</sub> in authentic fog water. *Science*. 260 (1993) 71-73.
- 373 [3] Y.G. Zuo, J. Hoigne, Formation of hydrogen peroxide and depletion of oxalic acid in  
374 atmospheric water by photolysis of iron(III)-oxalato complexes. *Environ. Sci.*  
375 *Technol.* 26 (1992) 1014-1022.
- 376 [4] D.Panias, M. Taxiarchou, I. Douni, I. Paspaliaris, A. Kontopoulos, Thermodynamic  
377 analysis of the reactions of iron oxides: dissolution in oxalic acid. *Can. Metal. Quart.*  
378 35 (1996) 363-373.
- 379 [5] D. Panias, M. Taxiarchou, I. Paspaliaris, A. Kontopoulos, Mechanisms of dissolution  
380 of iron oxides in aqueous oxalic acid solutions. *Hydrometallurgy*. 42 (1996) 257-265.
- 381 [6] M.I. Litter, E.C. Baumgartner, G.A. Urrutla, M.A. Blesa, Photodissolution of iron  
382 oxides. 3. Interplay of photochemical and thermal processes in maghemite/carboxylic  
383 acid systems. *Environ. Sci. Technol.* 25 (1991) 1907-1913.
- 384 [7] C. Siffert, B. Sulzberger, Light-Induced dissolution of hematite in the presence of  
385 oxalate: a case study. *Langmuir*. 7 (1991) 1627-1634.

- 386 [8] B. Sulzberger, H. Laubscher, Reactivity of various types of iron(III) (hydr)oxides  
387 towards light-induced dissolution. *Marine Chem.* 50 (1995) 103-115.
- 388 [9] P. Mazellier, B. Sulzberger, Diuron degradation in irradiated, heterogeneous  
389 iron/oxalate systems: The rate-determining step. *Environ. Sci. Technol.* 35 (2001)  
390 3314-3320.
- 391 [10] F.B. Li, X.Z. Li, X.M. Li, T.X. Liu, J. Dong, Heterogeneous photodegradation of  
392 bisphenol A with iron oxides and oxalate in aqueous solution. *J. Colloid Interf. Sci.*  
393 311 (2007) 481-490.
- 394 [11] C.S. Liu, F.B. Li, X.M. Li, G. Zhang, Y.Q. Kuang, The effect of iron oxides and  
395 oxalate on the photodegradation of 2-mercaptobenzothiazole. *J. Mol. Catal.*  
396 *A-Chem.* 252 (2006) 40-48.
- 397 [12] X.G. Wang, C.S. Liu, X.M. Li, F.B. Li, S.G. Zhou, Photodegradation of  
398 2-mercaptobenzothiazole in the  $\gamma$ -Fe<sub>2</sub>O<sub>3</sub>/oxalate suspension under UVA light  
399 irradiation. *J. Hazard. Mater.* 153 (2008) 426-433.
- 400 [13] Q. Lan, F.B. Li, C.S. Liu, X.Z. Li, Heterogeneous Photodegradation of  
401 Pentachlorophenol with Maghemite and Oxalate under UVA Illumination. *Environ.*  
402 *Sci. Technol.* 42 (2008) 7918-7923.
- 403 [14] D.L. Sedlak, J. Hoigné, The role of copper and oxalate in the redox cycling of iron  
404 in atmospheric waters. *Atmos. Environ.* 27A (1993) 2173-2185.
- 405 [15] H. Liu, C. Wang, X. Li, X. Xuan, C. Jiang, H. Hui, A Novel electro-Fenton process  
406 for water treatment: reaction-controlled pH adjustment and performance assessment.  
407 *Environ. Sci. Technol.* 41 (2007) 2937-2942.
- 408 [16] A. Safazadeh-Amiri, J.R. Bolton, S.R. Cater, Ferrioxalate-mediated  
409 photodegradation of organic pollutants in contaminated water. *Water Res.* 31 (1997)  
410 787-798.
- 411 [17] Y.G. Zuo, J. Zhan, Effects of oxalate on Fe-catalyzed photooxidation of dissolved



412 sulfur dioxide in atmospheric water. *Atmos. Environ.* 39 (2005) 27-37.

413 [18] B.C. Faust, R.G. Zepp, Photochemistry of aqueous iron(III)-polycarboxylate  
414 complexes: roles in the chemistry of atmospheric and surface waters. *Environ. Sci.*  
415 *Technol.* 27 (1993) 2517-2522.

416 [19] J.S. Jeong, J.Y. Yoon, pH effect on OH radical production in photo/ferrioxalate  
417 system. *Water Res.* 39 (2005) 2893-2900.

418 [20] F. Wu, N. Deng, Y. Zuo, Discoloration of dye solutions induced by solar photolysis  
419 of ferrioxalate in aqueous solutions. *Chemosphere.* 39 (1999) 2079-2085.

420 [21] X. Wang, L. Zhang, Y. Ni, J. H, X. Cao, Fast Preparation, characterization, and  
421 property study of  $\alpha$ -Fe<sub>2</sub>O<sub>3</sub> nanoparticles via a simple solution-combusting method.  
422 *J. Phys. Chem. C.* 113 (2009) 7003-7008.

423 [22] J. Yu, X. Yu, B. Huang, X. Zhang, Y. Dai, Hydrothermal synthesis and visible-light  
424 photocatalytic activity of novel cage-like ferric oxide hollow spheres. *Cryst.*  
425 *Growth Des.* 9 (2009) 1474-1480.

426 [23] J. Yu, G. Wang, B. Cheng, M. Zhou, Effects of hydrothermal temperature and time  
427 on the photocatalytic activity and microstructures of bimodal mesoporous TiO<sub>2</sub>  
428 powders. *Appl. Catal. B: Environ.* 69 (2007) 171-180.

429 [24] M. Zhou, J. Yu, B. Cheng, Effects of Fe-doping on the photocatalytic activity of  
430 mesoporous TiO<sub>2</sub> powders prepared by an ultrasonic method. *J. Hazard. Mater.* 137  
431 (2006) 1838-1847.

432 [25] F.B. Li, X.Z. Li, C.S. Liu, T.X. Liu, Effect of alumina on photocatalytic activity of  
433 iron oxides for bisphenol A degradation. *J. Hazard. Mater.* 149 (2007) 199-207.

434 [26] F.B. Li, X.G. Wang, Y.T. Li, C.S. Liu, F. Zeng, L.J. Zhang, M.D. Hao, H.D. Ruan,  
435 Enhancement of the reductive transformation of pentachlorophenol by  
436 polycarboxylic acids at the iron oxide-water interface. *J. Colloid Interf. Sci.* 321  
437 (2008) 332-341.

- 438 [27] M.A. Oturan, N. Oturan, C. Lahitte, S. Trevin, Production of hydroxyl radicals by  
439 electrochemically assisted Fenton's reagent: Application to the mineralization of an  
440 organic micropollutant, pentachlorophenol. *J. Electroanal. Chem.* 507 (2001)  
441 96-102.
- 442 [28] M. Fukushima, K. Tatsumi, K. Morimoto, Influence of iron(III) and humic acid on  
443 the photodegradation of pentachlorophenol. *Environ. Toxicol. Chem.* 19 (2000)  
444 1711-1716.
- 445 [29] M. Fukushima, K. Tatsumi, Degradation pathways of pentachlorophenol by  
446 photo-Fenton systems in the presence of Iron(III), humic Acid, and hydrogen  
447 peroxide. *Environ. Sci. Technol.* 35 (2001) 1771-1778.
- 448 [30] R.Z. Chen, J.J. Pignatello, Role of Quinone Intermediates as Electron Shuttles in  
449 Fenton and Photoassisted Fenton Oxidations of Aromatic Compounds. *Environ. Sci.*  
450 *Technol.* 31 (1997) 2399-2406.
- 451 [31] F. Chen, W.H. Ma, J.J. He, J.C. Zhao, Fenton degradation of malachite green  
452 catalyzed by aromatic additives. *J. Phys. Chem. A.* 106 (2002) 9485-9490.
- 453 [32] R. Augusti, A.O. Dias, L.L. Rocha, R.M. Lago, Kinetics and mechanism of benzene  
454 derivative degradation with Fenton's reagent in aqueous medium studied by MIMS.  
455 *J. Phys. Chem. A.* 102 (1998) 10723-10727.
- 456 [33] R.W. Matthews, The reaction chemistry of aqueous ferrous sulfate solutions at  
457 natural pH. *Aust. J. Chem.* 36 (1983) 1305-1317.
- 458 [34] T.E. Graedel, M.L. Mandich, Kinetic model studies of atmospheric droplet  
459 chemistry 2. Homogeneous transition metal chemistry in raindrops. *Geophys. Res.*  
460 91 (1986) 5205-5221.
- 461 [35] J. He, W.H. Ma, J.J. He, J.C. Zhao, J.C. Yu, Photooxidation of azo dye in aqueous  
462 dispersions of  $H_2O_2/\alpha\text{-FeOOH}$ . *Appl. Catal. B: Environ.* 39 (2002) 211-220.
- 463 [36] S. Banwart, S. Davies, W. Stumm, The role of oxalate in accelerating the reductive

464 dissolution of hematite ( $\alpha\text{-Fe}_2\text{O}_3$ ) by ascorbate. *Colloid and Surface*. 39 (1989)  
465 303-309.  
466

467 **Figure Captions**

468

469 **FIGURE 1.** The photodegradation of PCP versus reaction time in irradiated  
470 heterogeneous systems with  $0.4 \text{ g L}^{-1}$  iron oxides and different  $C_{\text{ox}}^0$  at initial pH 3.5: (A)  
471  $\alpha\text{-FeOOH}$  suspension; (B)  $\alpha\text{-Fe}_2\text{O}_3$  suspension. The inserted plot shows the dependence  
472 of the first-order rate constant ( $k$ ) of PCP degradation on  $C_{\text{ox}}^0$ .

473

474 **FIGURE 2.** The changes of dechlorination during PCP photodegradation in irradiated  
475 heterogeneous system with  $0.4 \text{ g L}^{-1}$  iron oxides and different  $C_{\text{ox}}^0$  at initial pH 3.5: (A)  
476  $\alpha\text{-FeOOH}$  suspension; (B)  $\alpha\text{-Fe}_2\text{O}_3$  suspension.

477

478 **FIGURE 3.** Detoxification of PCP during the reaction time at the optimal  $C_{\text{ox}}^0$  (1.2 mM)  
479 in  $\alpha\text{-FeOOH}$  and  $\alpha\text{-Fe}_2\text{O}_3$  systems under UVA illumination.

480

481 **FIGURE 4.** Concentration changes of PCP intermediates versus reaction time at the  
482 optimal  $C_{\text{ox}}^0$  (1.2 mM) in  $\alpha\text{-FeOOH}$  and  $\alpha\text{-Fe}_2\text{O}_3$  systems under UVA illumination. (A)  
483 *p*-chloranil; (B) HCOOH.

484

485 **SCHEME 1.** The mechanism of iron cycling with iron oxides and oxalate under UVA  
486 illumination in the presence of PCP. HQ and Q represent the hydroquinone  
487 (TeCC/TeCHQ) and quinone (*o*-chloranil/*p*-chloranil) intermediates detected. SQ  
488 represents the tetrachloro-*o*-semiquinone/tetrachloro-*p*-semiquinone radicals.

489

490 **FIGURE 5.** The concentration variation of adsorbed/dissolved Fe during PCP  
491 photodegradation for different  $C_{\text{ox}}^0$  in  $\alpha\text{-FeOOH}$  and  $\alpha\text{-Fe}_2\text{O}_3$  systems. (A) the adsorbed  
492 Fe(III); (B) the adsorbed Fe(II); (C) the dissolved Fe(III); (D) the dissolved Fe(II).

493

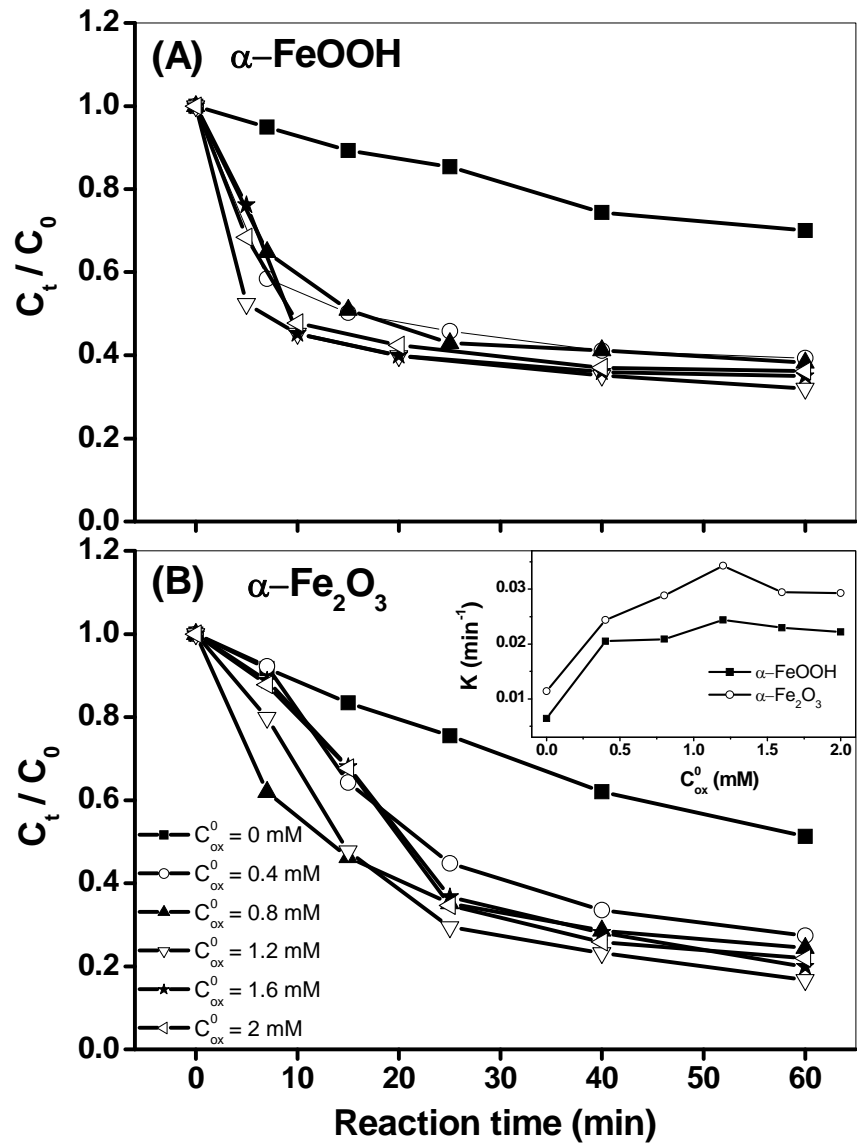
494 **FIGURE 6.** The formation of  $\text{H}_2\text{O}_2$  during PCP degradation in irradiated heterogeneous  
495 system with  $0.4 \text{ g L}^{-1}$  iron oxides and different  $\text{C}_{\text{ox}}^0$  at initial pH 3.5. (A)  $\alpha\text{-FeOOH}$   
496 system; (B)  $\alpha\text{-Fe}_2\text{O}_3$  system.

497

498

FIGURE 1

499



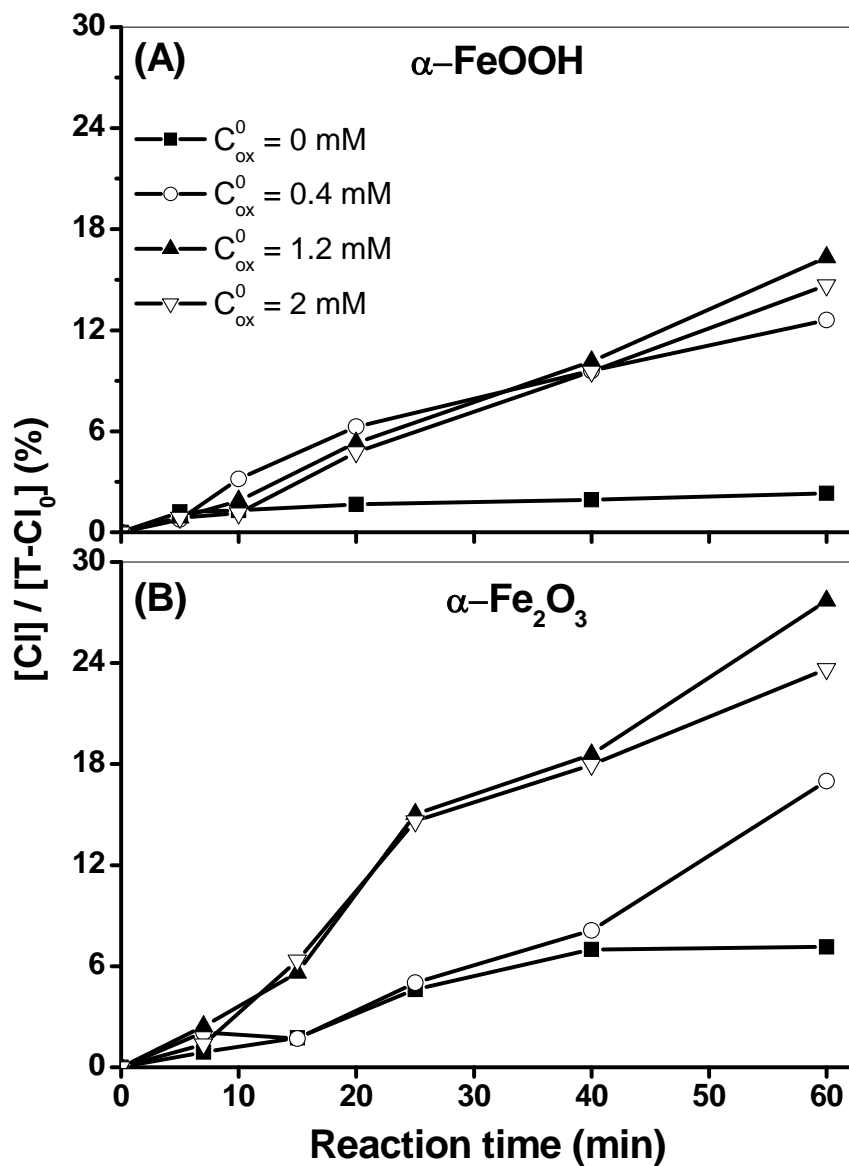
500

501

502

FIGURE 2

503



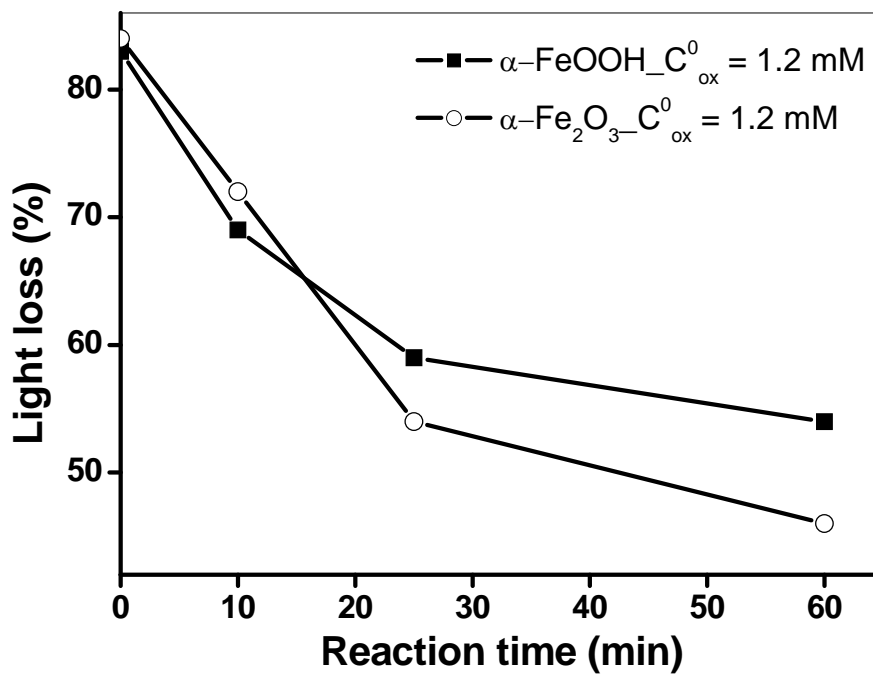
504

505

506

FIGURE 3

507



508

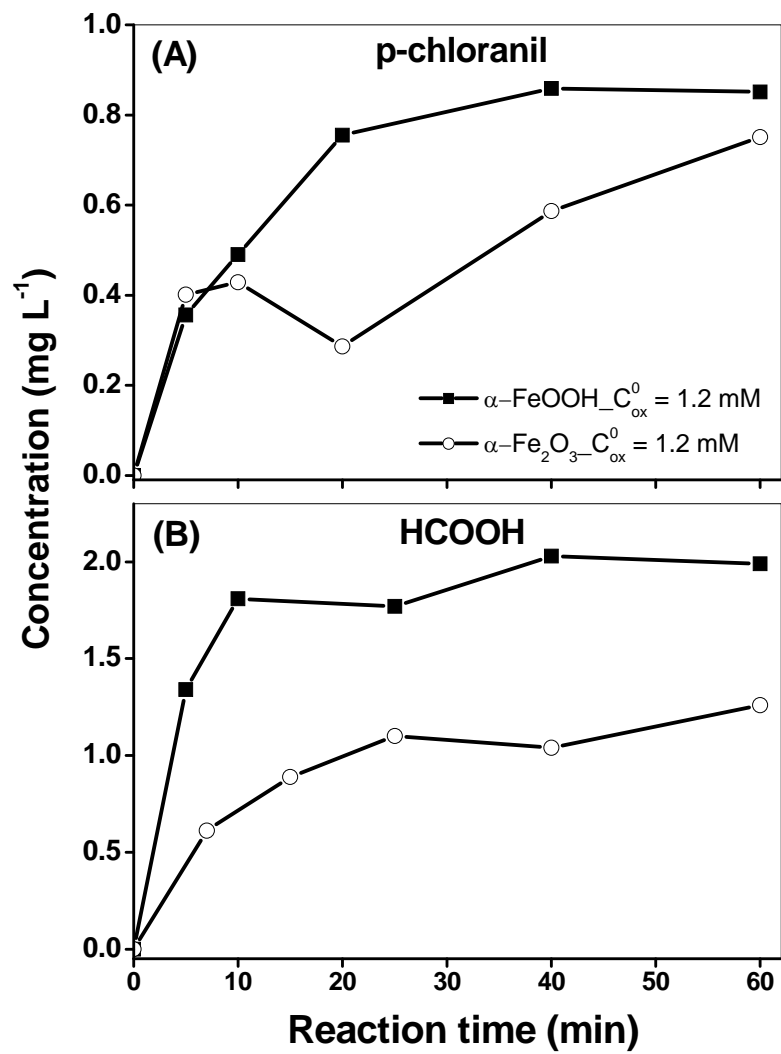
509



510

FIGURE 4

511

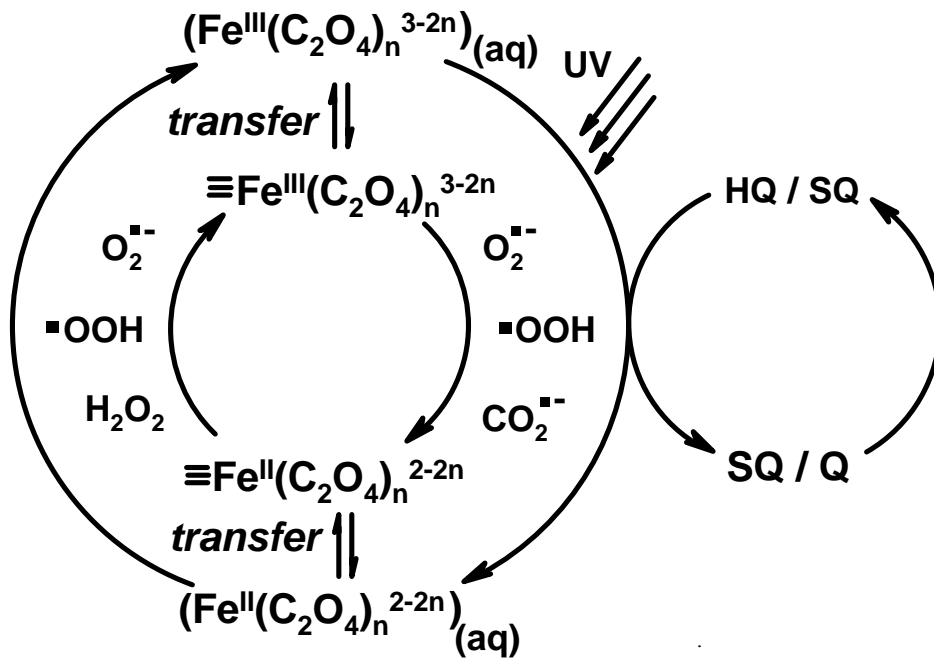


512

513

### SCHEME 1

514



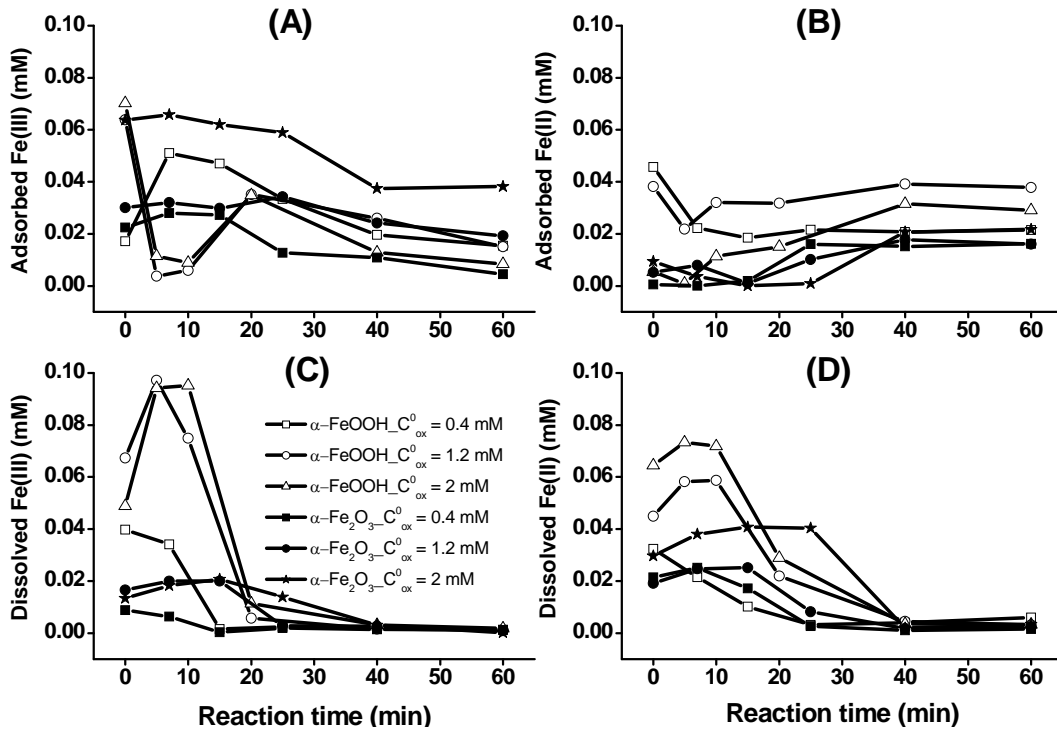
515

516

517

FIGURE 5

518



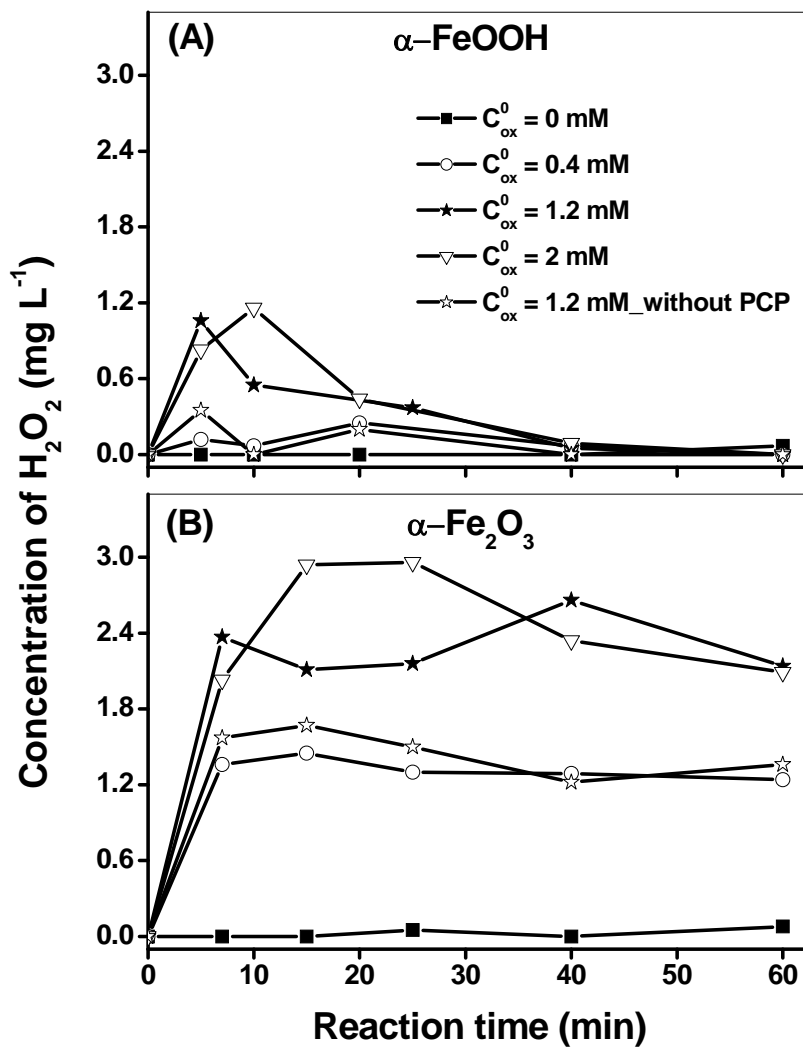
519

520

521

522

FIGURE 6



523